# *Extraordinary Transmission Characteristics of Subwavelength Nanoholes with Rectangular Lattice*



**Citation:** Cetin, Arif E., et al. "Extraordinary Transmission Characteristics of Subwavelength Nanoholes with Rectangular Lattice." Plasmonics, vol. 12, no. 3, June 2017, pp. 655–61.

**As Published:** https://doi.org/10.1007/s11468-016-0311-5

**Publisher:** Springer US

**Persistent URL:** http://hdl.handle.net/1721.1/116740

**Version:** Author's final manuscript: final author's manuscript post peer review, without publisher's formatting or copy editing

# Extraordinary Transmission Characteristics of Subwavelength Nanoholes with Rectangular Lattice

Arif E. Cetin[1], Martin Dršata[2], Yasa Ekşioğlu[3] and Jiří Petráček[2,4]

[1] Koch Institute for Integrative Cancer Research, Massachusetts Institute of Technology, Cambridge, MA 02139, USA

[2] Brno University of Technology, Faculty of Mechanical Engineering, Institute of Physical Engineering, Technická 2, 616 69 Brno, Czech Republic

[3] Istanbul Kemerburgaz University, Department of Electrical and Electronics Engineering, Bağcılar 34217, Istanbul, Turkey

[4] Brno University of Technology, CEITEC - Central European Institute of Technology, Technická 10, 616 00 Brno, Czech Republic

E-mail: petracek@fme.vutbr.cz

**Abstract**

We investigate the extraordinary light transmission (EOT) properties of nanohole arrays with rectangular lattice for label-free refractive index sensing applications. We show that the deviation within the periodicities along the two axes at the nanohole plane leads to more advantageous spectral quality of EOT signal compared to the conventional square lattice geometries. We introduce a way to further improve the sensitivity of the aperture system by carefully choosing the periodicities. We introduce nanohole arrays with rectangular lattice supporting EOT signals with larger figure-of-merit values as well as enabling much stronger light transmission. We also model a nanohole system covered with a thin dielectric layer, mimicking biomolecules captured on the gold surface, in order to show its biosensing capability. We also show that certain deviation amounts between periodicities create spectral splitting within the EOT signal leading to larger spectral shifts in the presence of a thin dielectric film.

**Keywords:** plasmonics, nanoholes, extraordinary light transmission, rectangular lattice, label-free biosensing

## 1. Introduction

Extraordinary optical transmission (EOT) through subwavelength nanohole arrays perforated through thin metallic films [1-4] took significant attention due to their tremendous optical properties advantageous for label-free biosensing [5-9]. The diffraction properties of nanoholes allow excitation

of surface plasmons (SPs), which leads to strong light transmission through the conversion of surface waves to light radiation at the nanohole exit, observed as peaks within the transmission spectra [1,2]. As SPs are trapped at the metal surface, i.e., propagating SP or surface plasmon polariton (SPP), as well as localized at metallic features, i.e., localized SP (LSP), they are very sensitive to change in the local refractive index. Hence, the variations within the refractive index in the vicinity can be used for real-time monitoring of binding events of biomolecules [10-12]. Consequently, different particle or aperture based plasmonic platforms have been introduced for biosensing applications [5-9,13-19]. In particular, periodic nanohole arrays appeal many researchers as they can combine the strength of localized and propagating surface plasmons.

For the biodetection configurations utilizing nanohole arrays, sensitivity depends on the hole diameter, array periodicity and the metal properties. Conventional nanohole systems utilize a square lattice geometry [5,6,12], where the periodicity along the two axes at the plane of apertures are symmetric. Recently, nanohole sensors with hexagonal lattice have been shown, which could further improve the sensing performance [20-22]. Utilizing a rectangular lattice geometry on the other hand, where the periodicity along *x*- and *y*-axes are distinct and thus the lattice exhibits polarization dependent properties, could add another mechanism to adjust the sensitivity character of the nanohole system [23].

In this paper, we investigate optical and sensing properties of nanohole arrays with rectangular lattice geometry. Contrary to the technique based on balanced intensity detection between two orthogonal polarizations of input beam [23], we rely on a more common approach where the incident light is linearly polarized in direction of one lattice vector. We show that the deviation from the square lattice could lead spectral "splitting" of EOT resonances, where the strength of splitting could be adjusted by changing the periodicity along one direction. We investigate the sensing properties of nanohole systems, where the apertures are embedded in a bulk solution as well as covered with a thin dielectric layer, mimicking a biomolecules captured on the sensing surface. We demonstrate that the spectral splitting in the rectangular lattice could lead much larger spectral shifts compared to the square lattice geometry.

## 2. Structure and methods

Fig. 1a shows the schematic illustration of the nanohole array with rectangular lattice. Here, $a_x$ and $a_y$ are the periods along *x*- and *y*-axes. Subwavelength holes are realized through a three-layered structure consisting of gold (Au), titanium (Ti) and silicon nitride (SiN). This configuration is similar to the previously demonstrated nanohole systems [6,24]. The spectral position of EOT resonances can be estimated by considering the excitation of SPPs (or SPP-like modes in the case of a dielectric film on a gold surface) at normal incidence via grating coupling. EOT signals excited through different grating orders, labeled with (*m*, *n*) along the *x*- and *y*-directions, are approximately located at wavelengths [23]

$$\lambda_{\text{res}} = \left( \frac{m^2}{a_x^2} + \frac{n^2}{a_y^2} \right)^{-1/2} \sqrt{\frac{\varepsilon_m + n_d^2}{\varepsilon_m n_d^2}} \tag{1}$$

where $a_x$ and $a_y$ are the periodicities along $x$- and $y$-directions, $\varepsilon_m$ is the permittivity of the metal and $n_d$ is the refractive index of the surrounding medium. For normally incident light source polarized along the $x$-direction, (0, $n$) modes are subradiant as they are weakly coupled to continuum, whereas ($m$, 0) modes are superradiant [6]. In our analyses we focus on the mode where $m$ = 1 and $n$ = 0, i.e., Au/Medium(1,0), as it is the most sensitive transmission resonance [12]. In this formulation, Medium refers to the medium in the vicinity of the aperture, overlapping with the evanescent tails of the SP waves. We calculate the transmission response of the nanohole arrays with rigorous finite difference time domain (FDTD) simulations. In simulations the mesh size is chosen as 5 nm along all directions. The dielectric functions of gold and titanium are taken from [25] and the refractive index of silicon nitride is set to 2.16.

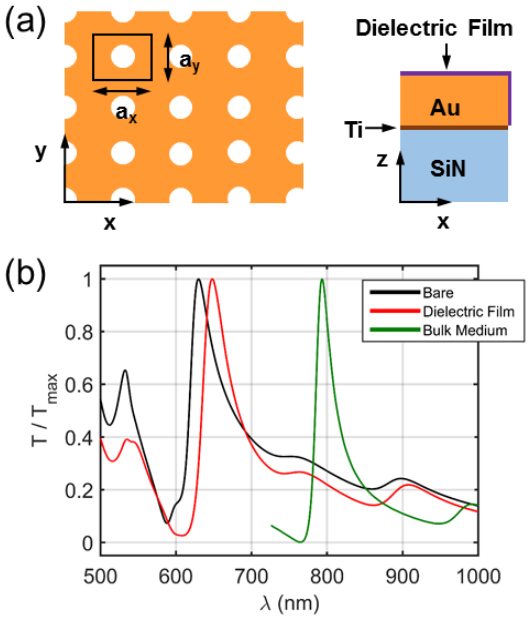


**Fig. 1 a** Top view and cross-section of the nanohole array with a rectangular lattice. The cross-sectional profile shows the dielectric film only covering the gold surface, which mimics an analyte captured on the Au surface. The array has periods $a_x$ and $a_y$ along the $x$- and $y$-directions. **b** Transmission $T$ (normalized to the maximum value, $T_{\text{max}}$) vs. wavelength $\lambda$ for the bare nanohole system (black line) and for systems after the addition of a 10 nm thick dielectric film (red line) and bulk medium (green line). The device parameters are: hole radius = 100 nm, array periodicity, $a_x$ = $a_y$ = 540 nm, and thicknesses of Au, Ti, and SiN layers are 120 nm, 5 nm and 70 nm, respectively. The refractive indices of the dielectric film and the bulk medium are 1.6 and 1.33, respectively.

In order to show the typical behavior of Au/Medium(1,0) mode, we first consider nanoholes arranged in a square lattice format with periods $a_x = a_y = 540$ nm. Fig. 1(b) shows the transmission spectra of the bare nanohole system (black line, Medium = air), the one after the addition of a dielectric film with refractive index, $n = 1.6$, only covering the gold surface which mimics an analyte captured on the Au surface (red line, Medium = the medium consisting of the dielectric film and air) and after immersing the whole nanohole system into a bulk medium with refractive index, $n_d = 1.33$ (green line, Medium = bulk medium). Initially, the EOT signal spectrally locates at 629.8 nm and shifts to 647.9 nm and 793.2 nm after the addition of dielectric layer and bulk medium due to the increase in local refractive index.

## 3. Results and discussion

In this section, we investigate the effect of periods $a_x$ and $a_y$ on the optical response of the nanohole array with a rectangular lattice. For an incident light, polarized along the *x*-direction, the spectral position of Au/Medium(1,0) mode is mainly determined by $a_x$, which can be inferred from equation (1) for $n = 0$. Consequently, a rectangular lattice with periods $a_x$ and $a_y$ is expected to exhibit similar spectral properties to a square lattice with period $a_x$. However, as we will show in the next section, by defining a deviation from the square lattice, both linewidth and spectral position of Au/Medium(1,0) mode could be fine-tuned. Here, we define a new parameter $\delta = a_y - a_x$, which determines the deviation from the square lattice. In consecutive steps, we investigate the effect of $\delta$ on the optical and sensing performances of, (i) bare nanohole system, (ii) the system embedded in bulk medium and (iii) the system covered with a dielectric film.

### 3.1. Bare nanohole array

Fig. 2a and 2b show the transmission spectra of the bare nanohole array for different $\delta$ values, where the period along *x*-axis is kept constant at $a_x = 540$ nm. When $\delta$ increases from negative to positive values, the peak transmission significantly drops and the resonance wavelength, initially located at $\lambda_{1res} \approx 625$ nm for $\delta = -90$ nm, gradually moves towards longer wavelengths (in Fig. 2a, the trend is marked with an arrow). Approximately for $\delta > 10$ nm, we observe another transmission peak at smaller wavelengths $\lambda_{2res} < \lambda_{1res}$, e.g., $\lambda_{2res} \approx 610$ nm for $\delta = 20$ nm. Further increasing $\delta$ significantly enhances the transmission at $\lambda_{2res}$ and shifts it towards longer wavelengths (in Fig. 2b, the trend is marked with an arrow). Finally, for $\delta > 50$ nm, the peak at $\lambda_{1res}$ disappears and we only observe a single peak at $\lambda_{2res}$. For any $\delta$, the peak at $\lambda_{2res}$ is always shifted to shorter wavelengths with respect to the position of the initial peak $\lambda_{1res}$ (e.g., $\lambda_{2res} \approx 618$ nm for $\delta = 90$ nm in Fig. 2b while $\lambda_{1res} \approx 625$ nm for $\delta = -90$ nm in Fig. 2a).

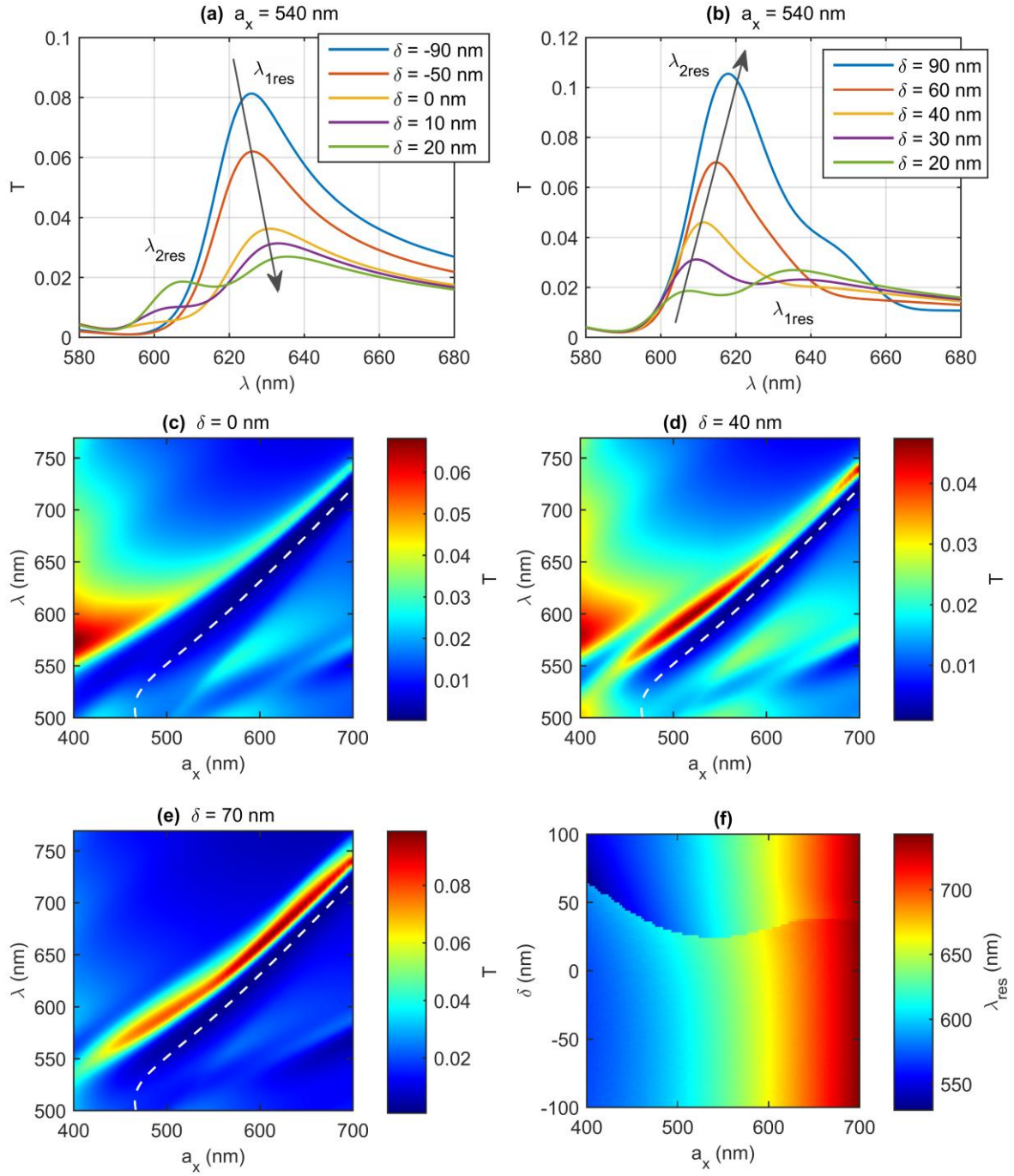


**Fig. 2** Optical characteristics of the bare nanohole array. **a**, **b** Transmission spectra ($T$) for different $\delta$ values, where the periodicity along $x$-direction $a_x$ = 540 nm. In figures, the arrows indicate the trend within the peak transmission of the corresponding resonances at $\lambda_{1res}$ and $\lambda_{2res}$ with $\delta$. **c**, **d**, **e** Color maps showing the transmission as a function of wavelength $\lambda$ and period $a_x$ for different $\delta$ values. The white dashed lines indicate the resonance position of the EOT signal calculated by equation (1). **f** Resonance wavelength $\lambda_{res}$ as a function of $a_x$ and $\delta$.

The overall behavior is summarized in Fig. 2c, 2d and 2e, showing transmission as a function of wavelength and period, $a_x$ for $\delta$ = 0, 40 nm and 70 nm. The resonance wavelength is mainly determined by $a_x$ and exhibits the trend predicted by equation (1) as depicted with a white dashed line in Fig. 2c, 2d and 2e. For square lattice $\delta$ = 0 (Fig. 2c) and for rectangular lattices with negative $\delta$ values, we observe only a single EOT peak (color maps for $\delta < 0$ look similar with the square lattice in Fig. 2c; therefore they are not presented). For $0 < \delta < 50$ nm, the EOT resonance becomes broader and "splits" into two distinct transmission resonances where such splitting is clearly seen in e.g., Fig. 2d, where $\delta$ = 40 nm and $a_x \approx 450$ nm. When $\delta$ is further increased, for $\delta > 50$ nm, the splitting disappears and the transmission spectra exhibit a single resonance (Fig. 2e). Fig. 2a - 2e also demonstrate that deviating from the square symmetry, i.e. increasing $|\delta|$ from zero, can significantly enhance peak transmission amplitude and could provide resonances with narrower linewidth. Fig. 2e indicates that large positive $\delta$ values can excite well-isolated EOT peaks, which would not spectrally overlap with other SP modes.

Fig. 2f shows the effect of $a_x$ and $\delta$ on the EOT resonance wavelength $\lambda_{res}$. For regions that exhibit the splitting, i.e., when both peaks at $\lambda_{1res}$ and $\lambda_{2res}$ are present, we choose the one with higher transmission. The discontinuity within the color map indicates the parameters $a_x$ and $\delta$ for which the peaks have the same transmission. Fig. 2f also shows that the distance between the peaks ("splitting strength") at the discontinuity, $\lambda_{1res} - \lambda_{2res}$, decreases with $a_x$ and eventually disappears. Consequently, no splitting phenomenon is observed for sufficiently high $a_x$ or $\lambda_{res}$.

### 3.2. Bulk sensor

In this section, we investigate the effect of $\delta$ on the sensitivity performance of the nanohole arrays embedded in a bulk medium with a refractive index $n_d$. The sensing capability of the apertures is determined by two parameters [8]: (i) bulk sensitivity, defined as the rate at which the resonance wavelength of the EOT resonance ($\lambda_{res}$) shifts with respect to the change in the refractive index of the bulk medium ($\Delta n_d$), $S = \Delta\lambda_{res} / \Delta n_d$, and (ii) figure-of-merit defined as the ratio between sensitivity and the EOT linewidth (FWHM), FOM = $S$ / FWHM, which is an asset to consider the spectral properties of such system in addition to its sensing capability.

Fig. 3 presents the dependence of $S$, FWHM and FOM on $\delta$ at $a_x$ = 500 nm. For the system immersed in water ($n_d$ = 1.33), the corresponding EOT peak is located at $\lambda_{res} \approx 750$ nm and the resonance splitting is no longer observed (transmission spectra is not shown here). As shown in the previous section, the effect of $\delta$ on optical sensing properties weakens with $a_x$; therefore, for the analysis in this section we choose a relatively small value of $a_x$, e.g., $a_x$ = 500 nm.

Deviating from the square lattice, i.e., by increasing $|\delta|$, decreases sensitivity (Fig. 3a), as well as narrows the EOT linewidth (Fig. 3b). The sensor performance determined by FOM could be easily seen by concurrently considering sensitivity and linewidth. For instance, using a rectangular lattice with negative $\delta$ could significantly increase FOM compared to the corresponding square lattice (Fig.

3c). Moreover, such lattice geometry offers larger transmission (not shown here), which could be highly advantageous for biodetection platforms utilizing imaging based devices.

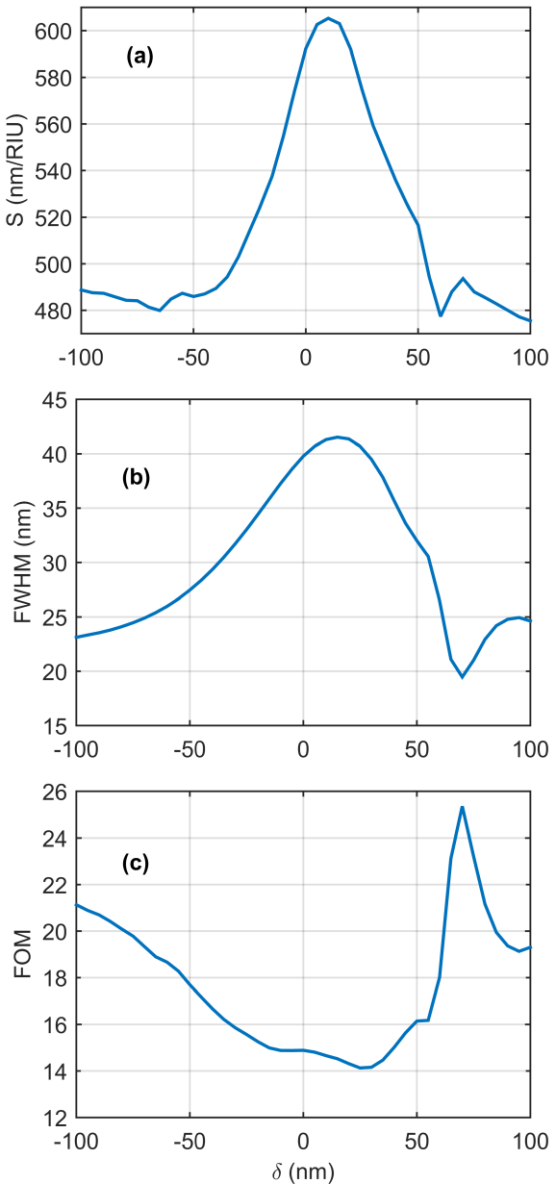


**Fig. 3 a** Sensitivity *S*, **b** FWHM and **c** FOM of the bulk sensor vs. $\delta$ at $a_x$ = 500 nm, where the aperture system is embedded in a media with $n_d$ = 1.33.

### 3.3. Surface sensor

In Fig. 4, we investigate the effect of $a_x$ and $\delta$ on the performance of the surface sensor. Fig. 4a shows the change in the EOT resonance wavelength ($\Delta\lambda_{res}$) due to the addition of a 10 nm dielectric layer on the Au surface. The most prominent feature is the presence of two discontinuities. The discontinuity located at lower $\delta$ corresponds to the resonance splitting for the bare system observed in Fig. 2f while the one at larger $\delta$ is given by the splitting for the system with the dielectric film. Between these two limits, there is a region of ($a_x$, $\delta$) pairs providing the largest spectral shift, which is due to the spectral

splitting. In biodetection platforms, the presence of the biomolecules is determined by monitoring the change in the resonance wavelength of the mode of interest, i.e., the one with the highest transmission. Therefore, for our rectangular aperture system within this region, the spectral shift due to the dielectric film is much larger compared to a system with a single EOT resonance since in the presence of the resonance splitting, the resonance with the highest transmission is observed at shorter wavelengths ($\lambda_{2res}$),while after addition of the dielectric film, the resonance with the highest transmission is observed now at longer wavelengths ($\lambda_{1res}$). Therefore, the total shift within the EOT resonance is further increased. On the other hand, the resonance splitting widens the linewidth, which could lower $\Delta\lambda_{res}$ / FWHM ratio as shown in Fig. 4b. Considering both refractive index sensitivity and linewidth of EOT resonances, the range with the highest $\Delta\lambda_{res}$ / FWHM ratio, i.e. $a_x$ > 480 nm and $\delta$ ~ 40 nm, could give an ideal nanohole platform with rectangular lattice for label-free biosensing applications.

Fig. 4a also shows that for ($a_x$, $\delta$) pairs which are not located between the two discontinuities, $\Delta\lambda_{res}$ behaves as in the case of the square lattice. However, as we observe in sections 3.1 and 3.2, decreasing $\delta$ from zero to large negative values can improve quality of the resonance, i.e., transmission efficiency and the linewidth. Fig. 4b shows that this effect is the strongest for $a_x$ ~ 550 nm, where we observe improvement in $\Delta\lambda_{res}$ / FWHM driven by narrowing FWHM.

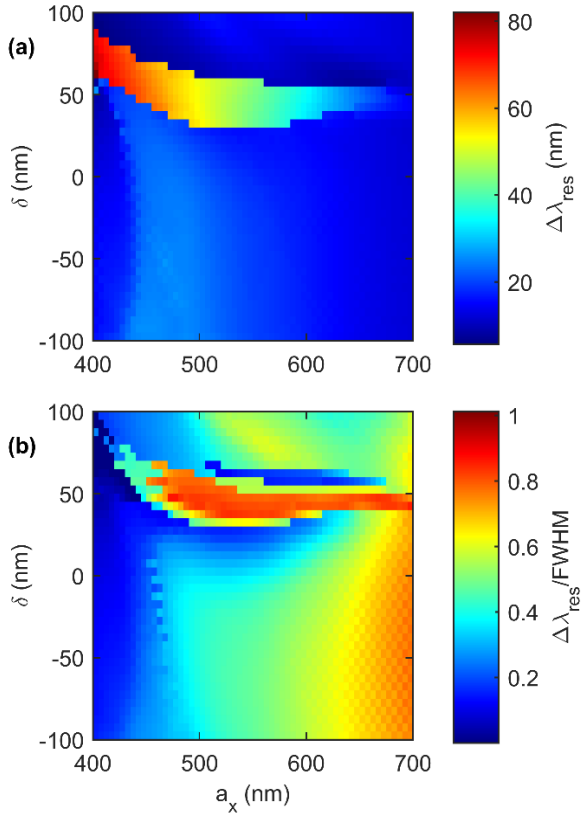


**Fig. 4 a** Shift in the EOT resonance wavelength $\Delta\lambda_{res}$ due to the 10 nm-thick dielectric film and **b** $\Delta\lambda_{res}$/FWHM ratio of the system after the addition of the dielectric layer as functions of period $a_x$ and period difference $\delta$.

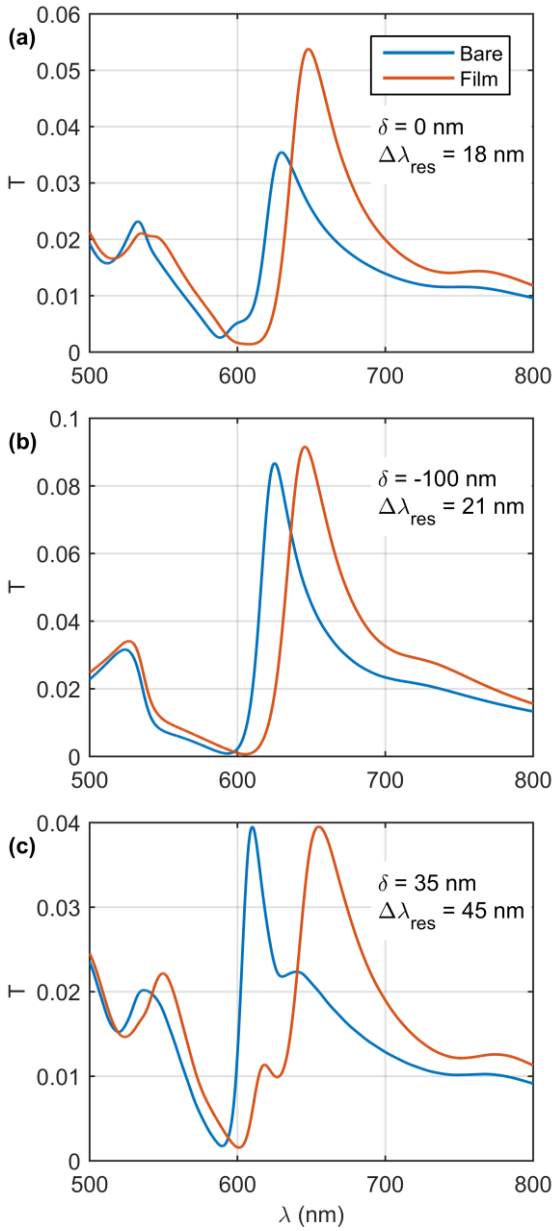


**Fig. 5** Transmission spectra ($T$) of the nanohole arrays before and after the addition a 10 nm-thick dielectric layer for period $a_x$ = 540 nm at **a** $\delta$ = 0 nm, **b** $\delta$ = -100 nm and **c** $\delta$ = 35 nm.

In Fig. 5, we gave specific examples to the features mentioned above. For a square lattice ($\delta$ = 0 in Fig. 5a), the addition of the dielectric layer shifts EOT resonance by 18 nm, while the linewidth of the transmission resonance is 58 nm. This gives us a $\Delta\lambda_{res}$ / FWHM ratio of 0.31. Using a large negative $\delta$ value, i.e., -100 nm (Fig. 5b), nanohole array supports a narrower EOT signal with linewidth of 46 nm as well as an improved sensitivity, i.e., 21 nm spectral shift due to the dielectric film. Hence, we have much larger $\Delta\lambda_{res}$ / FWHM ratio with the rectangular lattice, e.g., 0.45 compared to the square one.

This sensitivity could be further enhanced by utilizing a rectangular lattice with $\delta$ values, where we observe resonance splitting within the EOT signal. Fig. 5c shows the transmission spectra of the aperture system with $\delta$ = 35 nm. Before the addition of the dielectric film, the nanohole system

supports two distinct spectral features within the EOT signal due to the resonance splitting. After the addition of the dielectric film, the spectral feature with strong transmission is significantly suppressed, while the weaker one supports much larger light transmission. Here, as we monitor the resonance wavelength of the corresponding spectral feature with the largest transmission, we obtain as large as 45 nm shift within the EOT signal. For this configuration, even though we have a relatively wider EOT linewidth, 58 nm, our sensitivity compensates this problem, leading to a much larger $\Delta\lambda_{res}$ / FWHM = 0.77.

## 4. Conclusion

We theoretically investigated EOT responses of nanohole arrays with a rectangular lattice for label-free refractive index sensing applications. Compared to square lattice geometries, the asymmetry within the periodicity along two axes, determined with a parameter $\delta$, can significantly improve spectral quality of EOT signal, i.e., transmission efficiency and the linewidth. We show that by careful selecting of $\delta$ values, bulk sensing capability of such aperture systems can be significantly improved. For large negative $\delta$ values, FOM and transmission efficiency are stronger compared to the sensors with the square lattice. We also modeled a nanohole system covered with a thin dielectric layer, mimicking biomolecules captured on the gold surface. We show that within a narrow positive $\delta$ value range, the nanohole system supports larger spectral shifts due to the resonance splitting within the EOT signal. We believe that our work could provide an effective way to select the most advantageous lattice configuration to realize biodetection platforms providing the highest sensitivities.

## Acknowledgments

J. Petráček acknowledges the support of Ministry of Education, Youth, and Sports of the Czech Republic (project LD14008).

## References

[1] Ebbesen TW, Lezec HJ, Ghaemi HF, Thio T, Wolff PA (1998) Extraordinary optical transmission through sub-wavelength hole arrays. Nature 391:667–669

[2] Ghaemi HF, Thio T, Grupp DE, Ebbesen TW, Lezec HJ (1998) Surface plasmons enhance optical transmission through subwavelength holes. Phys Rev B 58:6779–6782

[3] Degiron A, Ebbesen TW (2005) The role of localized surface plasmon modes in the enhanced transmission of periodic subwavelength apertures. J Opt A Pure Appl Opt: 7 S90-S96

[4] Genet C, Ebbesen TW (2007) Light in tiny holes. Nature 445:39-46

[5] Brolo G, Gordon R, Leathem B, Kavanagh KL (2004) Surface plasmon sensor based on the enhanced light transmission through arrays of nanoholes in gold films. Langmuir 20:4813–4815

[6] Yanik AA, Cetin AE, Huang M, Artar A, Mousavi SH, Khanikaev A, Connor JH, Shvets G and Altug H (2011) Seeing protein monolayers with naked eye through plasmonic fano resonances. Proc Natl Acad Sci USA 108:11784-11789

[7] Chang T Y, Huang M, Yanik AA, Tsai HY, Shi P, Aksu S, Yanik MF, Altug H (2011) Large-scale plasmonics microarrays for label-free high-throughput screening. Lab Chip 11:3596–3602

[8] Valsecchi C, Brolo AG (2013) Periodic metallic nanostructures as plasmonic chemical sensors. Langmuir 29:5638-5649

[9] Monteiro JP, Carneiro LB, Rahman MM, Brolo AG, Santos MJL, Ferreira J, Girotto EM (2013) Effect of periodicity on the performance of surface plasmon resonance sensors based on subwavelength nanohole arrays. Sens Actuator B-Chem 178:366-370

[10] Cetin AE, Coskun AF, Galarreta BC, Huang M, Herman D, Ozcan A and Altug H (2014) Handheld high-throughput plasmonic biosensor using computational on-chip imaging. Light Sci Appl 3:1-10

[11] Coskun AF, Cetin AE, Galarreta BC, Alvarez DA, Altug H, Ozcan A (2014) Lensfree optofluidic plasmonic sensor for real-time and label-free monitoring of molecular binding events over a wide field-of-wiew. Sci Rep 4:1-7

[12] Cetin AE, Etezadi D, Galarreta BC, Busson MP, Eksioglu Y, Altug H (2015) Plasmonic nanohole arrays on a robust hybrid substrate for highly sensitive label-free biosensing. ACS Photonics 2:1167-1174

[13] Osawa M, Ikeda M (1991) Surface-enhanced infrared absorption of p-nitrobenzoic acid deposited on silver island films: contributions of electromagnetic and chemical mechanisms. J Phys Chem 95: 9914–9919

[14] Knepp K, Wang Y, Kneipp H, Perelman LT, Itzkan I, Dasari RR, Field MS (1997) Single molecule detection using surface-enhanced raman scattering (SERS). Phys Rev Lett 78:1667–1670

[15] Aksu S, Cetin AE, Adato R and Altug H (2013) Plasmonically enhanced vibrational biospectroscopy using low-cost infrared antenna arrays by nanostencil lithography. Adv Opt Mater 1**:**798–803

[16] Kabashin AV, Evans P, Pastkovsky S, Hendren W, Wurtz GA, Atkinson R, Pollard R, Podolskiy VA, Zayats AV (2009) Plasmonic nanorod metamaterials for biosensing. Nat Mater 8**:**867–871

[17] Artar A, Yanik AA, Altug H (2009) Fabry–Pérot nanocavities in multilayered plasmonic crystals for enhanced biosensing. Appl Phys Lett 95**:**051105

[18] Cetin AE, Altug H (2012) Fano resonant ring/disk plasmonic nanocavities on conducting substrates for advanced biosensing. ACS Nano 6:9989–9995

[19] Im H, Bantz KC, Lee SH, Johnson TW, Haynes CL, Oh SH (2013) Self-assembled plasmonic nanoring cavity arrays for SERS and LSPR biosensing. Adv Mater 25:2678–2685

[20] Thio T, Ghaemi HF, Lezec HJ, Wolff PA and Ebbesen TW (1999) Surface-plasmon-enhanced transmission through hole arrays in Cr films. J Opt Soc Am B 16:1743–48

[21] Couture M, Liang Y, Poirier Richard HP, Faid R, Peng W, Masson JF (2013) Tuning the 3D plasmon field of nanohole arrays. Nanoscale 5**:**12399-12408

[22] Ekşioğlu Y, Cetin AE, Petráček J (2015) Optical response of plasmonic nanohole arrays: comparison of square and hexagonal lattices. Plasmonics doi:10.1007/s11468-015-0118-9

[23] Blanchard-Dionne AP, Guyot L, Patskovsky S, Gordon R, Meunier M (2011) Intensity based surface plasmon resonance sensor using a nanohole rectangular array. Opt Express 19:15041-15046

[24] Yanik AA, Kamohara O, Artar A, Geisbert TW, Connor JH, Altug H 2010 An optofluidic nanoplasmonic biosensor for direct detection of live viruses from biological media. Nano Lett 10:4962–4969

[25] Hanes WM (2015) CRC Handbook of chemistry and physics. Boca Raton: CRC Press